Available online at www.sciencedirect.com
SCIENCE DIRECT®
Chemical Physics 296 (2004) 159–169
Chemical Physics
www.elsevier.com/locate/chemphys

Simulating spin-boson dynamics with stochastic Liouville–von Neumann equations ☆

Jürgen T. Stockburger *

Institut für Theoretische Physik II, Universität Stuttgart, Pfaffenwaldring 57, 70550 Stuttgart, Germany

Received 17 July 2003; accepted 17 September 2003

Abstract

Based on recently derived exact stochastic Liouville–von Neumann equations, several strategies for the efficient simulation of open quantum systems are developed and tested on the spin-boson model. The accuracy and efficiency of these simulations is verified for several test cases including both coherent and incoherent dynamics, involving timescales differing by several orders of magnitude. Using simulations with a time-dependent field, the time evolution of coherences in the reduced density matrix is investigated. Even in the case of weak damping, pronounced preparation effects are found. These indicate hidden coherence in the interacting system which can only be indirectly observed in the basis of the reduced quantum dynamics.

PACS: 03.65.Yz

Keywords: Spin-boson model; Stochastic Liouville–von Neumann equation; Open quantum system

1. Introduction

The model of a two-level atom interacting with a quantum field or many-particle reservoir has shown a remarkable persistence over decades of progress in physics, appearing and reappearing in many guises in different branches of condensed-matter physics after its 'first life' in quantum optics and magnetic resonance. It constitutes an idealized, minimal model of quantum dynamics and thermodynamics of *open* quantum systems. Through the explicit inclusion of a reservoir in the model, it supports the discussion of an open quantum system without resorting to speculative extensions of quantum mechanics.

The spin-boson problem [1–4] is fairly well understood for most parameter regimes relevant to solid-state physics, where the reservoir is characterized by a smooth spectral density running up to a large bandwidth cutoff, which enters the effective physics only as a renormalization parameter. A rich body of theoretical work on the spin-boson problem was developed in the context of macroscopic quantum coherence [5] and its realization in superconducting devices as well as the physics of defect tunneling in solids [6], to name two early examples. These results are currently being reapplied and extended in the discussion of performance limits of quantum computers, since the two-level atom of the spin-boson problem can obviously be identified with a qubit subject to a dephasing-inducing environment [7]. Apart from this general consideration, the spin-boson model also serves as a model for particular realizations, e.g., the flux qubit [8], where physical parameters can be given for the two-level system and its environment. Lastly, it should be mentioned that an intricate formal link has recently been pointed out [9,10] between the dynamics of the spin-boson model and both dissipative transport of light particles [11] in a periodic potential and transport of correlated electrons through a barrier in a 1D conductor [12].

☆ Dedicated to the 60th birthday of Ulrich Weiss.

* Fax: +49-711-685-4902.
E-mail address: stockburger@theo2.physik.uni-stuttgart.de (J.T. Stockburger).

0301-0104/$ - see front matter © 2003 Elsevier B.V. All rights reserved.
doi:10.1016/j.chemphys.2003.09.014

In the context of chemical physics, charge transfer and curve-crossing problems form an important context for the spin-boson problem. Here the understanding of the spin-boson dynamics seems less complete. The bandwidth of the dissipative reservoir may be small, or its spectrum may exhibit structured features relating to vibrational spectra. In addition to the energy scales of the two-level system and a damping constant, other parameters need to be considered. Moreover, the spin-boson treatment of chemical phenomena is often considered only a first approximation, since the linear-response assumption for the reservoir is inherent in the model; a generalization to non-linear, more complex reservoirs is sometimes warranted. Since there is no mature theory of non-linear reservoirs, the straightforward way to achieve such a generalization is the formal inclusion of key degrees of freedom of the reservoir, e.g., some prominent vibrational modes, in the open system. But even the spin-boson problem itself is not fully understood absent the scaling behavior found in solid-state physics.

It is not to be expected that a thorough theoretical treatment of the more complex models just indicated can be accomplished by analytic methods alone; numerical simulations will become more important as larger open systems are studied. Likewise, simulations are likely to help in charting the remaining *terra incognita* of the spin-boson problem, e.g., the electron transfer problem in the inverted regime. Future progress will place competing demands on numerical methods which most established algorithms cannot meet at the same time: acceptable scaling of computational complexity with *both* system size and time interval simulated [13]. Additionally, the method should take into account the generally non-Markovian nature of quantum fluctuations.

The usual starting point for the theoretical description of an open quantum system beyond perturbation theory, by now more or less canonical, uses the path integral formalism, which allows the exact treatment of quantum memory effects [14]. Since quantum memory effects do not allow the path integral to be translated into a simple differential equation of motion, this limits the choice of theoretical and numerical approaches available. The direct evaluation of path integrals using Monte Carlo sampling is a reliable method for short to intermediate times [15–17] but becomes prohibitively expensive at long times due to the dynamical sign problem. The recursive evaluation of a path integral using the quasiadiabatic path-integral discretization (QUAPI) allows propagation to arbitrarily long times, but needs computational resources which grow very rapidly with increasing system size or memory time [18–20].

More recently, stochastic approaches have allowed a transition from the path integral description to equations of motion [21–26]. Similar to the intuitive – and computationally advantageous – representation of classical dissipative systems through the motion of a phase-space point under the influence of thermal noise and friction, an open quantum system can be described by the stochastic propagation of pure quantum states [21–28]. Favorable scaling with system size seems an *intrinsic* feature common to these approaches – the computational complexity of the open-system simulation as a function of system size remains the same as that of simulating the same quantum system without external interaction. The remainder of this article is largely devoted to the question how the second objective, good scaling for long-time dynamics, can be achieved in the presence of memory effects. For tests of this performance aspect, the spin-boson system is a prime candidate, since comparison results are readily available.

A summary of the formal description of dissipative quantum systems through stochastic Liouville–von Neumann (SLN) equations given in Section 2 (see also [25,26]). Section 3 discusses new material, giving details of numerical approaches based on the SLN formalism. A series of numerical tests on the free dynamics of the spin-boson model as well as simulation results probing hidden coherence in the spin-boson model through pulsed external fields are presented in Section 4, followed by a summary of results and conclusions. Appendix A presents the derivation of a mathematical result needed in Section 2.

2. Stochastic Liouville–von Neumann equations for open quantum systems

Although a connection between the influence functional formalism and classical colored noise in quantum dynamics was pointed out already in the seminal work of Feynman and Vernon [14], it has been put to use in the theory and in simulations of open quantum systems only recently [21–26] (see, however, [29,30]). The key ideas of one such stochastic approach to open quantum systems [25,26] will be outlined in this section using a more general model than the spin-boson model, commonly known as the Caldeira–Legget model. The Caldeira–Legget model consists of a one-dimensional potential model coupled to a thermal reservoir of harmonic oscillators with a quasicontinuous distribution of frequencies

$$H = \frac{p^2}{2m} + V(q) + \sum_j \frac{m_j\omega_j^2}{2}\left(x_j - \frac{c_j}{m_j\omega_j^2}q\right)^2 + \frac{p_j^2}{2m_j}. \quad (1)$$

With the identification

$$\hat{q} \to \frac{q_0}{2}\sigma_z, \quad (2)$$

where q_0 is a characteristic length scale, the spin-boson Hamiltonian

$$H_{\rm SB} = -\frac{\hbar\Delta}{2}\sigma_x + \frac{\hbar\varepsilon}{2}\sigma_z - \frac{q_0}{2}\sigma_z\sum_j c_j x_j + \sum_j \frac{p_j^2}{2m_j} + \frac{m_j\omega_j}{2}x_j^2 \tag{3}$$

can be considered a truncation of the Caldeira–Legget model to two localized states [3,31].

The dynamics of the harmonic reservoir is usually of little interest; moreover, due to the large size of the total system, only a reduced description from which the oscillators have been eliminated is simple enough to be practically treatable. Although Master equations have been frequently been used with considerable success in weak-coupling scenarios such as quantum optics [32], a formally exact reduced formalism, usually necessary in a condensed-matter context, is known only in path integral formalism. Feynman and Vernon [14] have demonstrated that the path integral

$$\rho(q_{\rm f}, q'_{\rm f}; t) = \int {\rm d}q_{\rm i}\int {\rm d}q'_{\rm i}\int_{q_{\rm i}}^{q_{\rm f}} D[q_1]\int_{q'_{\rm i}}^{q'_{\rm f}} D[q_2] \times \exp\left(\frac{\rm i}{\hbar}(S_0[q_1] - S_0[q_2])\right) \times F[q_1 - q_2, (q_1+q_2)/2]\rho(q_{\rm i}, q'_{\rm i}; t_0) \tag{4}$$

is an exact expression for the time evaluation of the reduced density matrix $\rho(q_{\rm f}, q'_{\rm f}; t)$ for an initial density matrix which factorizes between $\rho(q_{\rm i}, q'_i; t_0)$ and a thermal density matrix of the harmonic reservoir. Here $S_0[q]$ denotes the classical action functional associated with the one-dimensional potential model. The influence functional

$$F[x,r] = \exp\left(-\frac{1}{\hbar}\Phi[x,r]\right) \tag{5}$$

with

$$\Phi[x,r] = \frac{1}{\hbar}\int_{t_0}^{t}{\rm d}t'\int_{t_0}^{t'}{\rm d}t'' x(t')\left[{\rm Re}L(t'-t'')x(t'') + 2{\rm i}\,{\rm Im}L(t'-t'')r(t'')\right] + \frac{{\rm i}\mu}{\hbar}\int_{t_0}^{t}{\rm d}t' x(t')r(t') \tag{6}$$

contains the full physics of the system–reservoir interaction and all aspects of the reservoir dynamics which may be reflected in the system dynamics. The kernel

$$L(t) = \frac{\hbar}{\pi}\int_0^\infty {\rm d}\omega J(\omega)\left(\coth\frac{\hbar\omega\beta}{2}\cos\omega t - {\rm i}\sin\omega t\right) \tag{7}$$

describes free fluctuations of the reservoir's coupling coordinate, themselves dependent on a spectral density $J(\omega)$ and inverse thermal energy β. Typical spectral densities in the context of solid-state physics are smooth in the relevant frequency regime, e.g., proportional to ω^3 for bulk phonons or of the Ohmic form $J(\omega) = \eta\omega$ for the low-energy excitations of a Fermi liquid. In the case of the spin-boson model, a dimensionless constant $\alpha = q_0^2\eta/(2\pi\hbar)$ describes the strength of Ohmic dissipation.

The last term in Eq. (6) has the form of a potential modification, which reflects the fact that the system–reservoir interaction given in Eq. (1) eliminates any quasistatic response of the reservoir; it relates to dynamic reservoir's dynamic response function $\chi_{\rm R}(t-t') = -2\Theta(t-t'){\rm Im}L(t-t')/\hbar$ through $\mu = \int_0^\infty {\rm d}\tau\,\chi_{\rm R}(\tau)$. This potential term has no effect for the spin-boson model, from $q^2 \equiv q_0^2/4$ one finds $\mu x r = (\mu/2)(q_1^2 - q_2^2) = 0$.

The path integral expression (4) has the distinct advantage of providing an exact description of the system-plus-reservoir dynamics which is reduced to only the system degree of freedom. However, the propagator for the reduced density matrix described by Eq. (4) is *not* associative due to the fact that the exponent of $F[x,r]$ contains a *double* time integral, i.e., there are memory effects which make quantum amplitudes a non-local functional on the path space.

At the price of introducing a further functional integral over auxiliary function spaces of complex functions $\xi(t)$ and $v(t)$, this non-locality can be lifted, representing the influence functional as a weighted average of quantum amplitudes containing a time-local action functional

$$F[x,r] = \int D^2[\xi]\int D^2[v]W[\xi,\xi^*,v,v^*] \times \exp\left(\frac{\rm i}{\hbar}\int_{t_0}^{t}{\rm d}t'\,\xi(t')x(t') + {\rm i}v(t')r(t')\right) \times \exp\left(-\frac{{\rm i}\mu}{\hbar}\int_{t_0}^{t}{\rm d}t' x(t')r(t')\right) \tag{8}$$

with a suitable Gaussian functional $W[\xi,\xi^*,v,v^*]$. Because W is normalized, it may be interpreted as a probability density of real noise fluctuations $(\xi+\xi^*)/2$, $(\xi-\xi^*)/(2{\rm i})$, $(v+v^*)/2$ and $(v-v^*)/(2{\rm i})$. It is partly characterized by the noise correlation functions

$$\langle\xi(t)\xi(t')\rangle_W = {\rm Re}L(t-t'), \tag{9}$$

$$\langle\xi(t)v(t')\rangle_W = (2{\rm i}/\hbar)\Theta(t-t'){\rm Im}L(t-t') = -{\rm i}\chi_{\rm R}(t-t'), \tag{10}$$

$$\langle v(t)v(t')\rangle_W = 0 \tag{11}$$

required for the identification of Eqs. (8) and (5). W is also characterized by the correlations $\langle\xi(t)\xi^*(t')\rangle$, $\langle\xi(t)v^*(t')\rangle$ and $\langle v(t)v^*(t')\rangle$, which do not enter the physical result obtained upon stochastic averaging.

The immediate benefit of the stochastic construction (8) becomes clear if the order of the integrations over (q, q') and (ξ, v) is interchanged: for any specific functions $\xi(t)$ and $v(t)$ the path-integral dynamics can be translated into the Schrödinger picture in the usual way. Observing that the exponents in Eq. (8) can be identified as action functionals associated with a time-dependent potential, we immediately recover the equation of motion

$$\mathrm{i}\hbar\dot{\rho} = [H_0, \rho]_- - \xi(t)[q, \rho]_- + \frac{\mu}{2}[q^2, \rho]_- - \frac{\hbar}{2}v(t)[q, \rho]_+, \tag{12}$$

a stochastic Liouville–von Neumann equation. The presence of both complex parameters and an anticommutator makes this equation describe a non-unitary propagation of individual samples, allowing ρ to acquire a non-hermitean component. After stochastic averaging, however, any non-hermitean parts of ρ vanish. Similarly, the trace of ρ varies between individual samples, but remains equal to unity on average.

This diffusive spread of the sample trace can be reduced or eliminated by introducing a 'guide trajectory' (to be specified later) in the anticommutator term

$$\mathrm{i}\hbar\dot{\hat{\rho}} = [H_0, \hat{\rho}]_- - \xi(t)[q, \hat{\rho}]_- + \frac{\mu}{2}[q^2, \hat{\rho}]_- - \frac{\hbar}{2}v(t)[q - \bar{r}_t, \hat{\rho}]_+ \tag{13}$$

where

$$\rho(t) = \exp\left(\mathrm{i}\int_0^t \mathrm{d}t'\, v(t')\bar{r}_{t'}\right)\hat{\rho}(t) \tag{14}$$

relates $\hat{\rho}$ to the solution of the original Eq. (12) for arbitrary $\bar{r}_t$. It is to be noted that Eqs. (13) and (14) do not set the stage for an approximate expansion; together they form an exact identity. The guide trajectory may depend on the noise forces in the form of a functional $\bar{r}_t[\xi(t'), v(t')]$, where the following properties will be assumed:

$$\frac{\delta\bar{r}_t}{\delta\xi(t')} = 0, \quad t' \geqslant t, \tag{15}$$

$$\frac{\delta\bar{r}_t}{\delta v(t')} = 0, \quad t' \geqslant t, \tag{16}$$

$$\frac{\delta\bar{r}_t}{\delta\xi^*(t')} = 0 \quad \text{any } t', \tag{17}$$

$$\frac{\delta\bar{r}_t}{\delta v^*(t')} = 0 \quad \text{any } t'. \tag{18}$$

In words, the functional $\bar{r}_t[\xi(t'), v(t')]$ is required to be *causal* and *analytic*.

Under these conditions, the exponential factor in Eq. (14) can be absorbed into the probability measure by re-defining the center of the Gaussian functional $W[\xi, \xi^*, v, v^*]$ (see Appendix A). This leads to new noise forces with same variance but dynamically shifted mean values:

$$\xi_t(t') = \xi(t') - \mathrm{i}\int_0^t \mathrm{d}s\,\langle\xi(t')v(s)\rangle\bar{r}(s) = \xi(t') + \int_0^t \mathrm{d}s\,\chi_{\mathrm{R}}(t'-s)\bar{r}(s), \tag{19}$$

$$\xi_t^*(t') = \xi^*(t') - \mathrm{i}\int_0^t \mathrm{d}s\,\langle\xi^*(t')v(s)\rangle\bar{r}(s), \tag{20}$$

$$v_t(t') = v(t'), \tag{21}$$

$$v_t^*(t') = v^*(t') - i\int_0^t \mathrm{d}s\,\langle v^*(t')v(s)\rangle\bar{r}(s). \tag{22}$$

Dropping the subscript t after the transformation has been performed, we obtain the SLN equation

$$\mathrm{i}\hbar\dot{\hat{\rho}} = [H_0, \hat{\rho}]_- - \left(\xi(t) - \int_{t_0}^t \mathrm{d}t'\,\chi_{\mathrm{R}}(t-t')\bar{r}_{t'}\right)[q, \hat{\rho}]_- + \frac{\mu}{2}[q^2, \hat{\rho}]_- - \frac{\hbar}{2}v(t)[q. - \bar{r}_t, \hat{\rho}]_+, \tag{23}$$

to be averaged with the *original* probability density $W[\xi, \xi^*, v, v^*]$ without the exponential factor of Eq. (14).

A natural choice for $\bar{r}_t$ relates it to the dynamics on the time interval $[0, t]$

$$\bar{r}_t = \frac{\mathrm{tr}\, q\rho(t)}{\mathrm{tr}\,\rho(t)} = \mathrm{tr}\, q\hat{\rho}(t). \tag{24}$$

Since this makes Eq. (23) conserve the trace of $\hat{\rho}$ for each sample, we call Eq. (23) a *normalized* SLN equation for a guide trajectory defined by Eq. (24). Compared to the linear SLN equation (12) the normalized version allows a more efficient stochastic averaging as well as a clear interpretation of the classical limit of Eq. (23) [25,26].

The implementation of a numerical simulation algorithm based on the normalized SLN equation is now relatively straightforward. For a numerical construction of the noise fluctuations, ξ is decomposed into a purely real $\xi^{(\mathrm{l})}$ with a long autocorrelation timescale, which is uncorrelated to all other noise forces, and a short-range complex part $\xi^{(\mathrm{s})}$, with correlations:

$$\left\langle\xi^{(\mathrm{l})}(t)\xi^{(\mathrm{l})}(t')\right\rangle = \mathrm{Re}\,L(t-t'), \tag{25}$$

$$\left\langle\xi^{(\mathrm{s})}(t)\xi^{(\mathrm{s})}(t')\right\rangle = 0, \tag{26}$$

$$\left\langle\xi^{(\mathrm{s})}(t)v(t')\right\rangle = -\mathrm{i}\chi_{\mathrm{R}}(t-t'), \tag{27}$$

$$\left\langle\xi^{(\mathrm{s})}(t)v^*(t')\right\rangle = 0, \tag{28}$$

$$\left\langle v(t)v(t')\right\rangle = 0. \tag{29}$$

Here the correlations of $\xi^{(s)}$ and v decay rapidly for $\omega_c|t-t'| \gg 1$, while correlations of $\xi^{(I)}(t)$ persist up to the thermal timescale $\hbar\beta$.

These noise fluctuations are generated numerically with great efficiency by filtering white noise with suitable integral operators, whose kernels have spectra which multiply to yield the spectra of $L(t-t')$ and $\chi_R(t-t')$. The necessary convolution operations can be performed with ease using a fast Fourier transform algorithm. This construction also determines the non-physical correlations $\langle \xi^{(s)}(t)\xi^{(s)*}(t')\rangle$ and $\langle v(t)v^*(t')\rangle$.

The non-linearity of the numerically simulated dynamics can be reduced by observing that the solution of the *simplified* SLN equation

$$\mathrm{i}\hbar\dot{\rho} = [H_0,\rho]_- - \left(\xi(t) - \int_{t_0}^{t} \mathrm{d}t'\,\chi_R(t-t')\bar{r}_{t'}\right)[q,\rho]_- + \frac{\mu}{2}[q^2,\rho]_- - \frac{\hbar}{2}v(t)[q,\rho]_+ \tag{30}$$

immediately yields a solution of the non-linear SLN equation (23) through the relation

$$\hat{\rho}(t) = \frac{1}{\operatorname{tr}\rho(t)}\rho(t). \tag{31}$$

A further simplification of Eq. (30) lies in the factorizing ansatz $\rho = |\psi_1\rangle\langle\psi_2|$, which reduces Eq. (30) to the two Schrödinger equations

$$\mathrm{i}\hbar|\dot{\psi}_1\rangle = H_0|\psi_1\rangle - \left(\xi(t) - \int_{t_0}^{t} \mathrm{d}t'\,\chi_R(t-t')\bar{r}_{t'}\right)q|\psi_1\rangle + \frac{\mu}{2}q^2|\psi_1\rangle - \frac{\hbar}{2}v(t)q|\psi_1\rangle, \tag{32}$$

$$\mathrm{i}\hbar|\dot{\psi}_2\rangle = H_0|\psi_2\rangle - \left(\xi^*(t) - \int_{t_0}^{t} \mathrm{d}t'\,\chi_R(t-t')\bar{r}^*_{t'}\right)q|\psi_2\rangle + \frac{\mu}{2}q^2|\psi_2\rangle + \frac{\hbar}{2}v^*(t)q|\psi_2\rangle. \tag{33}$$

Apart from the satisfaction of arriving at a conceptually simple result from an involved mathematical transformation, this reflects very positively on the scaling of stochastic simulations: for a single noise sample, the numerical effort of propagating the system scales with system size exactly the same way as for a conservative system. Moreover, it is interesting to note that Eqs. (32) and (33) capture all effects of the system–reservoir interaction, including quantum correlations and entanglement between system and reservoir, through the addition of *single-particle* operators to the Hamiltonian H_0. The description of quantum dissipation through single-particle operators strongly suggests that a wide range of approximations to conservative quantum systems (e.g., formalisms suitable for large atoms or small molecules) can be combined with this stochastic approach. Larger and more complex quantum systems, which can currently be simulated only under the assumption of energy conservation, are likely to become accessible to an open-system approach using SLN equations. There is an attractive feature in in the SLN approach which may recommend it for complex systems even in the case of very weak damping, where perturbative methods are valid: Whereas Born–Markov perturbative approaches such as Redfield equations define damping in terms of system *and* reservoir characteristics, often making reference to an exact diagonalization of the system, the SLN noise terms are constructed from the free *reservoir* dynamics alone; no characteristics of the free system dynamics enter the formal description of dissipation.

3. Optimized stochastic simulation methods

For the transformed noise forces given in Eqs. (15)–(18) the linear combinations $\xi_t \pm \xi_t^*$ and $v_t \pm v_t^*$ are no longer purely real or purely imaginary. The transformed integration measure is formally Gaussian, but the integration, even when written over the real components of ξ and v, is shifted in the complex domain. However, the stochastic simulation of Eq. (30) must use real-valued components for these shifted quantities, i.e., the numerical simulation of Eq. (30) operates on an analytic continuation of the exact result. Although this continuation is known to be free of singularities in important cases such as the classical limit, the weak-coupling limit and any harmonic system, the spin-boson model (at low temperature) appears to be a counterexample where the simulation becomes unstable after returning excellent results up to a well-defined time threshold t_c, which is related to the growth of the non-hermitean part of $\hat{\rho}$. Beyond the threshold a sudden onset of peak-like artefacts and other systematic errors is observed, in close similarity to stability problems found in the Master equations for the positive P function, a quantum optical phase space function [33,34]. As in the latter example, SLN simulations using Eq. (30) are highly accurate for times below the threshold time. In the light of these facts two natural ways to extend the power of the SLN methodology are: (a) increasing the timescale t_c and (b) finding consistent methods to 'reshuffle' the ensemble to a healthy state before artefacts taint the data.

3.1. Alternative noise spectra

In the scaling limit any relevant frequency Ω of the dissipative dynamics lies within the band of reservoir frequencies, $\Omega \ll \omega_c$, i.e., the complex noise forces, which drive the system away from normalized hermitean states, act on the system at resonance. This can be changed if the potential term in the influence functional is formally included in the stochastic construction, which leads to modified cross-correlations for the noise fluctuations $\xi^{(s)}$ and v

$$\left\langle \xi^{(s)}(t)v(t')\right\rangle = -\mathrm{i}\chi_{\mathrm{R}}(t-t') + \mathrm{i}\mu\delta(t-t'). \tag{34}$$

Instead of a noise spectrum extending roughly over the interval $[-\omega_c, \omega_c]$, we are now dealing with a white noise spectrum that has a *gap* in the same interval. The resonant driving of the system by complex noise is thus strongly reduced, typically increasing the critical time t_c by one or more orders of magnitude. With the proviso that increments of the white noise parts of ξ and v be interpreted in the sense of a Stratonovich stochastic integral, the steps taken in the derivation of Eqs. (23) and (30) can be reiterated unchanged. This yields

$$\mathrm{i}\hbar\dot{\rho} = [H_0,\rho]_- - \left(\xi(t) - \int_{t_0}^{t} \mathrm{d}t'\,\chi_{\mathrm{R}}(t-t')\bar{r}_{t'} + \mu\bar{r}_t\right)[q,\rho]_- - \frac{\hbar}{2}v(t)[q,\rho]_+ \tag{35}$$

as a modified version of the simplified SLN equation (30), which has the additional advantage of having only translationally invariant dissipation terms.

3.2. Collective normalization of subensembles

Next we consider the case of a subensemble of N samples $\rho^{(j)}(t)$, each governed by an independent set of noise forces $\xi^{(j)}(t)$, $v^{(j)}(t)$. In this case, a set of guide trajectories $\bar{r}_t^{(j)}$ can be given which does not conserve the trace of each sample, but only their sum. Again, guide trajectories enter an exponential factor distinguishing normalized and unnormalized states, but here a single factor is used for different noise realizations

$$\rho^{(j)}(t) = \prod_{k=1}^{N} \exp\left(\mathrm{i}\int_0^{t'} \mathrm{d}t'\,v^{(k)}(t')\bar{r}_t^{(k)}\right)\hat{\rho}^{(j)}(t) \tag{36}$$

with

$$\bar{r}_t^{(k)} = \frac{\mathrm{tr}\,q\rho^{(k)}(t)}{\sum_{l=1}^{N}\mathrm{tr}\,\rho^{(l)}(t)} = \frac{1}{N}\mathrm{tr}\,q\hat{\rho}^{(k)}(t). \tag{37}$$

For initially normalized states, this keeps the sum over traces identical to N.

Again, the exponential factors in Eq. (36) must be absorbed into the probability measure through suitable shifts of the noise fluctuations. Because the (unshifted) noises acting on different members of the subensemble are uncorrelated, and because terms with different $v^{(k)}$ in Eq. (36) factorize, the shifts of noise fluctuations ($\xi^{(j)}$, $\xi^{(j)*}$, $v^{(j)}$, $v^{(j)*}$) and ($\xi^{(k)}$, $\xi^{(k)*}$, $v^{(k)}$, $v^{(k)*}$) with $j \neq k$ are *independent* of each other. Thus the derivation presented in the Appendix A applies also in this case. Eq. (19) is only trivially modified for collectively normalized samples

$$\xi_t^{(j)}(t') = \xi^{(j)}(t') + \int_0^t \mathrm{d}s\,\chi_{\mathrm{R}}(t'-s)\bar{r}_t^{(j)}(s). \tag{38}$$

The corresponding normalized SLN equation reads

$$\mathrm{i}\hbar\dot{\hat{\rho}}^{(j)} = [H_0,\hat{\rho}^{(j)}]_- - \left(\xi^{(j)}(t) - \int_{t_0}^{t}\mathrm{d}t'\,\chi_{\mathrm{R}}(t-t')\bar{r}_{t'}^{(j)}\right) \times \left[q,\hat{\rho}^{(j)}\right]_- + \frac{\mu}{2}[q^2,\hat{\rho}]_- - \frac{\hbar}{2}v^{(j)}(t)\left[q,\hat{\rho}^{(j)}\right]_+ + \sum_{k=1}^{N}\hbar v^{(k)}(t)\bar{r}_t^{(k)}\hat{\rho}^{(j)}. \tag{39}$$

Again, there is a simplified SLN equation suitable for numerical simulation

$$\mathrm{i}\hbar\dot{\rho}^{(j)} = [H_0,\rho^{(j)}]_- - \left(\xi^{(j)}(t) - \int_{t_0}^{t}\mathrm{d}t'\,\chi_{\mathrm{R}}(t-t')\bar{r}_{t'}^{(j)}\right) \times \left[q,\rho^{(j)}\right]_- + \frac{\mu}{2}[q^2,\rho]_- - \frac{\hbar}{2}v^{(j)}(t)\left[q,\rho^{(j)}\right]_+, \tag{40}$$

related to the normalized form (39) by

$$\hat{\rho}^{(j)}(t) = \frac{N}{\sum_{k=1}^{N}\mathrm{tr}\,\rho^{(k)}(t)}\rho^{(j)}(t). \tag{41}$$

It is evident from Eq. (37) that $\bar{r}_t^{(j)}$ is of order $1/N$, i.e., the shift (and the corresponding non-linearity of the equation of motion) vanishes for large N; the threshold time t_c is thus further extended. The linear SLN equation (12) is recovered from (40) in the limit $N \to \infty$.

3.3. Separation of friction and thermal time scales

The split of ξ into the long- and short-range components $\xi^{(l)}$ and $\xi^{(s)}$ allows the numerical solution of SLN equations using a two-stage averaging procedure, which separates the difficulty of dealing with long-range correlations from the problems incurred through complex driving forces. In a primary averaging stage (inner sampling loop), samples are drawn for $\xi^{(s)}$ and v, while $\xi^{(l)}$ will be changed only in the secondary averaging stage (outer sampling loop). For simulation parameters yielding a sufficiently large threshold time, $\omega_c t_c \gg 1$, the short-time noise correlation $\langle\xi(t)v(t')\rangle$ can be block factorized on intervals of width $\tau < t_c$, as indicated in Fig. 1 (left). Under the condition $\omega_c\tau \gg 1$ this leaves the effective support of the correlator $\langle\xi(t)v(t')\rangle$ virtually untouched.

In the primary averaging, the dynamical simulation can thus be partitioned over finite time intervals, accumulating and then drawing new Hermitean samples at the end of each interval. This procedure does not disturb the long-time correlations since all samples drawn for the primary averaging evolve subject to the same realization of $\xi^{(l)}$. In the secondary averaging, the entire procedure is repeated for a sufficient number of long-range fluctuations $\xi^{(l)}$, which remain unconstrained in the t, t' plane. Their effective support forms a diagonal band of width $\propto \hbar\beta$ (Fig. 1, right).

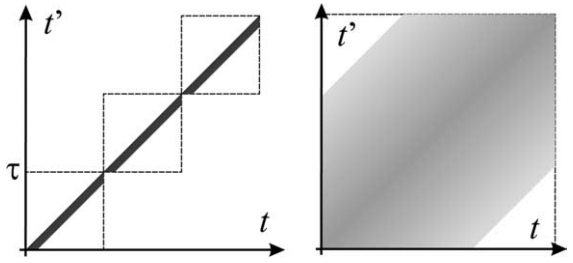

Fig. 1. Schematic representation of block factorization of short-time correlations (left) vs. global reach of long-time correlations (right) (see Section 3.3).

4. Tests and results for the spin-boson model

Numerical tests and applications of the simulation strategies described in Section 3 are discussed in the following; a combination of all three strategies is used unless indicated otherwise. The underlying SLN equations of motion for the spin-boson model are as follows: The linear SLN equation reads

$$\mathrm{i}\hbar\dot{\rho} = -\frac{\hbar\Delta}{2}[\sigma_x,\rho]_- + \frac{\hbar\varepsilon}{2}[\sigma_z,\rho]_- - \xi(t)[\sigma_z,\rho]_- - \frac{\hbar v}{2}[\sigma_z,\rho]_+. \tag{42}$$

Absent any physical context defining a characteristic length q_0, σ_z is identified with the position operator q. The normalized and simplified SLN equations are

$$\begin{aligned}\mathrm{i}\hbar\dot{\hat{\rho}} = &-\frac{\hbar\Delta}{2}[\sigma_x,\hat{\rho}]_- + \frac{\hbar\varepsilon}{2}[\sigma_z,\hat{\rho}]_- \\ &-\left(\xi(t) - \int_{t_0}^{t} \mathrm{d}t'\,\chi_{\mathrm{R}}(t-t')\bar{\sigma}_{t'}\right)[\sigma_z,\hat{\rho}]_- \\ &-\frac{\hbar v}{2}[\sigma_z-\bar{\sigma}_t,\hat{\rho}]_+ \end{aligned} \tag{43}$$

(with $\bar{\sigma}_t = \mathrm{tr}\,\sigma_z\hat{\rho}$) and

$$\begin{aligned}\mathrm{i}\hbar\dot{\rho} = &-\frac{\hbar\Delta}{2}[\sigma_x,\rho]_- + \frac{\hbar\varepsilon}{2}[\sigma_z,\rho]_- \\ &-\left(\xi(t) - \int_{t_0}^{t} \mathrm{d}t'\,\chi_{\mathrm{R}}(t-t')\bar{\sigma}_{t'}\right)[\sigma_z,\rho]_- \\ &-\frac{\hbar v}{2}[\sigma_z,\rho]_+ \end{aligned} \tag{44}$$

(with $\hat{\rho} = \rho/\mathrm{tr}\,\rho$), respectively. Throughout the following, Ohmic dissipation with an algebraic cutoff

$$J(\omega) = \frac{\eta\omega}{\left(1+\frac{\omega^2}{\omega_{\mathrm{c}}^2}\right)^2} \tag{45}$$

corresponding to an exponentially decaying response function

$$\chi_{\mathrm{R}}(t) = \mu\omega_{\mathrm{c}}^2 t\exp(-\omega_{\mathrm{c}}t) \tag{46}$$

is used.

4.1. Coherent dynamics: free oscillations

The coherent dynamics of the spin-boson model at moderate damping, $\alpha < 1/2$, and low temperature are theoretically well understood and numerically accessible using other methods, thus providing a suitable test case to verify the accuracy and stability of the SLN approach. Using data obtained through an established path-integral Monte Carlo (PIMC) method for comparison [15], the power and efficiency of the SLN approach in the region of coherent dynamics at zero temperature is demonstrated. Fig. 2 shows the time evolution of the expectation value $\langle\sigma_z\rangle$ of a symmetric system from an initially factorized state.

In the SLN approach the dynamics can be accurately simulated over many oscillation periods; empirical data suggest that the growth of statistical errors saturates to a constant value for increasing t, allowing the simulation to be continued to arbitrarily long times. This overcomes an inherent restriction of the PIMC approach, which suffers from the so-called dynamical sign problem. The PIMC approach mainly employs the superposition principle to obtain quantum amplitudes. The resulting averaging over highly oscillatory functions results in a signal-to-noise ration of the MC simulation which degrades exponentially with growing t, leading to near-divergent error estimates after about one oscillation period. For very strong system–reservoir coupling, however, quantum phase factors are suppressed, and the PIMC approach gains in efficiency.

The computer times of the SLN and PIMC simulations shown in Fig. 2 are comparable; they vary between 40 and 210 h on a commodity CPU (Athlon, 1200 MHz). The SLN simulations, whose statistical errors are

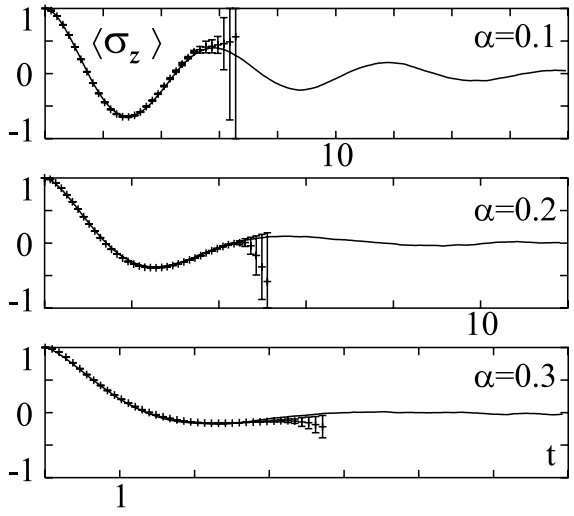

Fig. 2. Comparison of SLN simulation data (lines) and path-integral Monte Carlo data (symbols) for coherent spin-boson dynamics at zero temperature. The time t is scaled by the renormalized matrix element Δ_{r} (see text).

comparable to the linewidth, use between 10 and 20 factorization blocks. The time axis is scaled by the renormalized matrix element $\Delta_r = \Delta(\Delta/\omega_c)^{\alpha/(1-\alpha)}$. In the SLN simulations a high cutoff $\omega_c = 20\Delta$ was used while a lower cutoff $\omega_c = 6\Delta$ was used in the PIMC simulation to avoid ergodicity problems.

4.2. Incoherent relaxation: long-time dynamics

Simulating the slow exponential decay of localized populations in a biased spin-boson model, as it occurs, e.g., in electron transfer reactions, is chosen as another test case. For parameter regions with non-trivial transient behavior, an explicit simulation of time-dependent population numbers can offer advantages over simulations linking rates to thermal flux correlation functions [17]. The population difference $P(t)$ is chosen as a dynamical observable; $P(t)$ is formally defined as the time-dependent expectation value $\sigma_z(t)$ for a two-state system starting from the factorized initial state with

$$\rho(t=0) = \begin{pmatrix} 1 & 0 \\ 0 & 0 \end{pmatrix} \tag{47}$$

and the reservoir in thermal equilibrium. For rate calculations, it is essential that $P(t)$ can be simulated over a long enough time interval to be directly fitted to an exponential function. Since $P(t)$ decays towards a non-zero value in a biased system, it is advantageous to symmetrize it under a reversal of the bias sign, $\varepsilon \to -\varepsilon$, i.e., study

$$P_s(t) = \frac{1}{2}(P_\varepsilon(t) + P_{-\varepsilon}(t)). \tag{48}$$

Because changing the sign of ε is the same as interchanging the eigenstates of σ_z, this can be expressed as a single expectation value with an *antisymmetric* initial state

$$P_s(t) = \langle\sigma_z(t)\rangle, \quad \rho(t=0) = \frac{1}{2}\begin{pmatrix} 1 & 0 \\ 0 & -1 \end{pmatrix}. \tag{49}$$

Using this equivalent definition of the symmetrized expectation value $P_s(t)$ as the basis of numerical simulations,the data presented in Fig. 3 is obtained. Parameters are $\alpha = 0.1$, $\omega_c/\Delta = 100$, $k_BT/\hbar\Delta = 10$ and ε as indicated in the figure. Since the simulation time is many orders of magnitude longer than the inverse of ω_c, the relatively large number of 300 factorization blocks may be used. In spite of the large number of time steps, the computation of a single curve in Fig. 3 took only about 15 min.

For rates varying over more than an order of magnitude, a remarkably stable simulation result for exponential decay is found, extending over many time constants. Given the fact that these curves result from the averaging of *coherently* propagated samples, this is truly remarkable. In the light of this successful example of a highly efficient simulation, it is to be expected that more elaborate simulations using this technique will be powerful enough to generate benchmark data for electron transfer rates which can be used to check theoretical approximations.

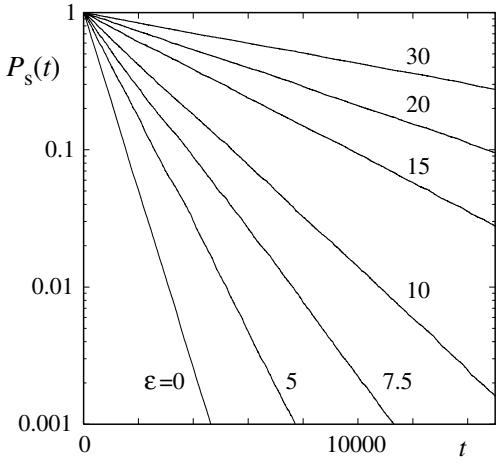

Fig. 3. Exponential relaxation of the asymmetric spin-boson system. All curves agree with analytic non-adiabatic rates within a few percent. The time t is given in units of Δ.

4.3. Rapid dephasing: short-time dynamics

The dephasing of a coherent superposition of quantum states is one of the fastest processes in spin-boson dynamics. It is mainly governed by the *interaction* part of the Hamiltonian (3) [35]. After preparing the system in an eigenstate of σ_x, again with a factorizing initial condition, dephasing expresses itself through the decay of the off-diagonal elements of the density matrix, here probed by measuring $\langle\sigma_x(t)\rangle$. The results given in Fig. 4 are for different values $\alpha = 5$, 2, 1, 0.5, 0.2, 0.1 and 0.05 of the dissipation constant (different symbols, from bottom left to top right).

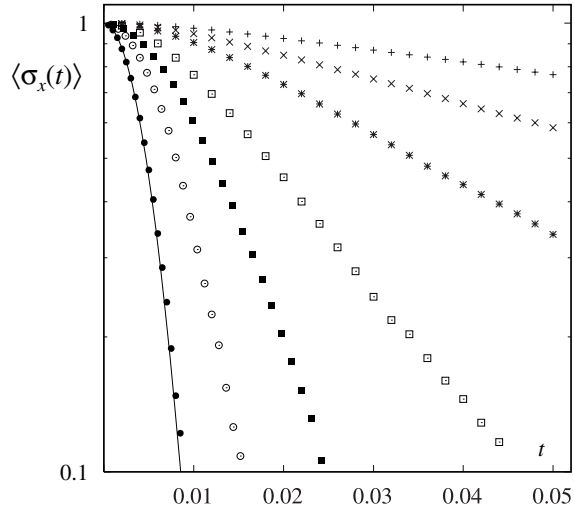

Fig. 4. Rapid decoherence of a symmetric superposition of localized states with a factorized initial density matrix and $\omega_c/\Delta = 100$, $k_BT/\hbar\Delta = 20$ and with α varying from 5 (symbol '●', curve at left) to 0.05 (symbol '+', at top). The time t is given in units of Δ.

As outlined in [35], a transition from a rapid Gaussian decay towards a slower, more complicated decay is observed when varying the damping constant from strong to weak damping. Excellent agreement between the analytic strong-coupling result (solid line) and simulation (filled dots) is observed. The statistical errors are less than ± 0.02.

4.4. Preparation effects: probing hidden coherence

In the case of moderate damping $\alpha < 1/2$ and low enough temperature, the initial rapid decay of a coherent superposition leads to a relaxed state with some residual coherence, which can be probed by time-dependent external fields. As is commonly done in elementary treatments of magnetic resonance, the reduced density matrix of the two-level system can be parameterized by a polarization or spin vector $\vec{M}$

$$\rho = \frac{1}{2}\left\{ \begin{pmatrix} 1 & 0 \\ 0 & 1 \end{pmatrix} + \vec{M}\cdot\vec{\sigma} \right\}, \tag{50}$$

where $\vec{M} \equiv \langle \vec{\sigma} \rangle$. Preparation of the two-state systems as a symmetric superposition of the eigenstates of σ_z corresponds to a spin vector of unit length pointing in the x-direction. Allowing the system to evolve from a factorized initial state (as in the previous subsection), the direction of $\vec{M}$ is conserved due to symmetry, while the reduction of its length indicates dephasing. In the case of weak damping, however, the initial dephasing saturates at a finite value of $\langle \sigma_x \rangle$. As shown in Fig. 5, this residual coherence can be probed through a pulsed external field in the z-direction, which changes the relative phase of the superposition, or, in other words, rotates the spin vector by an angle of $\pi/2$, leaving it antiparallel to the y-axis (without changing its norm). The following free dynamics displays damped Rabi oscillations resembling a precession of the spin vector. However, the norm $|\vec{M}| = \sqrt{\langle \sigma_x \rangle^2 + \langle \sigma_y \rangle^2 + \langle \sigma_z \rangle^2}$ of the spin vector does not fall monotonously, as one might expect for a dissipative system. After a quarter oscillation period $\vec{M}$ points in the z-direction, with M_z exceeding the relaxed value of $|\vec{M}|$ before the onset of oscillations. This indicates *hidden coherence* in the *interacting* system, which does not become visible in the reduced density matrix. Results for a delta-shaped pulse (solid line) and a finite-width pulse (dashed line), whose shape is indicated at the bottom of Fig. 5, are virtually identical.

To test this interpretation in terms of hidden coherence, the free decay of $\langle \sigma_z \rangle$ and $\langle \sigma_y \rangle$ is compared in Fig. 6 for the two different preparations of the initial state at $t = 0$. The rotated relaxed state (delta-pulse case of Fig. 5) is compared to the dynamics starting with a *factorized* initial state, where the reduced density matrix at $t = 0$ is identical in both cases. A significant preparation effect is found: In the factorized case, coherence appears to be drastically reduced compared to the initial preparation derived from a relaxed state, supporting the notion of hidden coherence. While a rapid initial dephasing is again

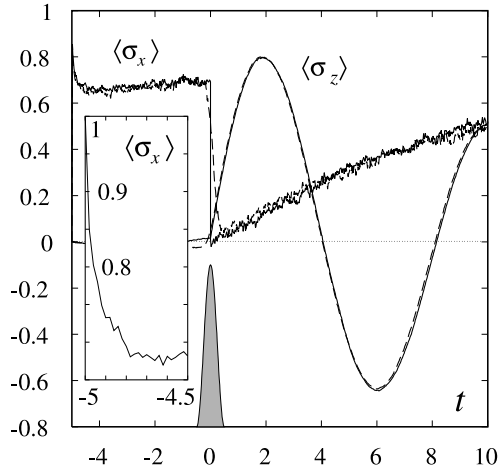

Fig. 5. Dynamical simulation with a symmetric superposition as an initial state (factorizing with the reservoir state). The relaxed state after a rapid initial dephasing (inset) is probed by a pulsed field in z-direction at $t = 0$, which rotates the spin vector by an angle of $\pi/2$. Subsequently, the residual coherence of the relaxed state reveals itself through oscillatory dynamics. The rise of $\langle \sigma_z \rangle$ *above* the relaxed value of $\langle \sigma_x \rangle$ is a counterintuitive observation, indicating that the quantity $\langle \sigma_x \rangle$ underestimates the coherence present in the interacting system. Solid lines indicate dynamics for a delta pulse at $t = 0$, dashed lines a finite-width pulse with equal area and shape as indicated in the figure. Parameters are $\Delta = 1$, $\omega_c = 250$, $\alpha = 0.05$ and $k_B T = 0$.

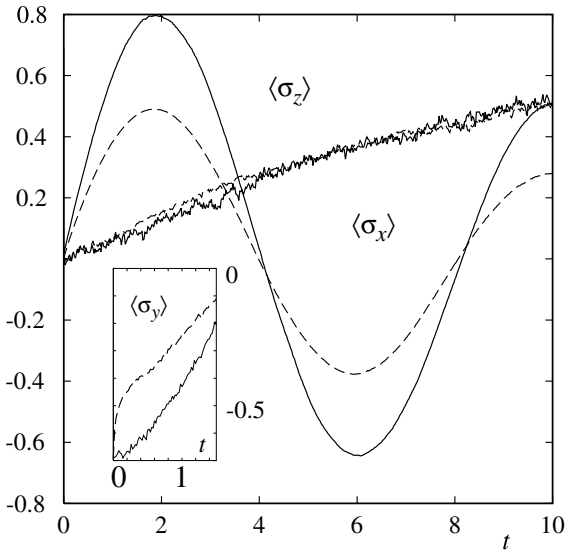

Fig. 6. Comparison of coherent oscillations starting from a relaxed delocalized state (solid lines, same as Fig. 5) and a factorized initial state at $t = 0$ with identical reduced density matrix ρ (dashed lines). A rapid initial decay of $\langle \sigma_y \rangle$ is observed for the factorized initial state, but not for the relaxed state, resulting in a significant difference in the amplitudes of coherent oscillations, while the expectation value $\langle \sigma_x \rangle$ seems to be unaffected by the choice of initial preparation. Parameters are $\Delta = 1$, $\omega_c = 250$, $\alpha = 0.05$ and $k_B T = 0$.

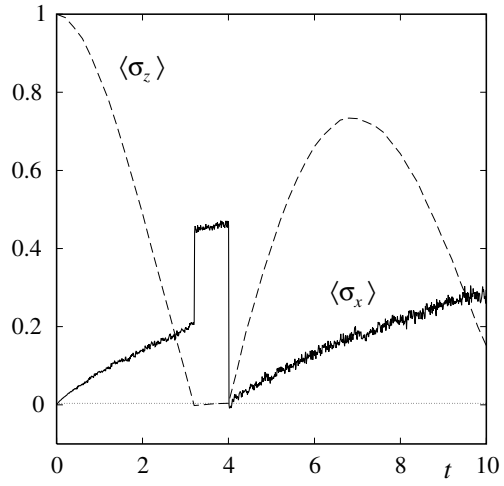

Fig. 7. Two-pulse dynamics revealing hidden coherence. After the free precession of the spin vector starting from a conventional localized/factorizing initial state, a pulsed field applied at $t = 3.2$ rotates the spin vector from the x–y-plane onto the x-axis. At $t = 4$, a second pulse rotates the spin vector onto the y-axis, allowing the free precession to resume. The amplitude of the following oscillations demonstrates that the value of $\langle\sigma_x\rangle$ observed between pulses significantly underestimates coherence. Parameters are $\Delta = 1$, $\alpha = 0.1$, $\omega_c/\Delta = 1000$ and $k_B T = 0$.

observed for the factorizing initial state, it appears to be absent for the relaxed preparation (see inset of Fig. 6).

Signatures of hidden coherence can be observed without taking a symmetric state for a starting point. Fig. 7 shows a simulation starting from a conventional factorized preparation involving a localized state, which has been commonly used as a standard in the spin-boson literature. After a quarter-period of free oscillatory dynamics, a pulsed field in z-direction rotates the spin vector to align it with the x-direction, effectively stopping the precession of $\vec{M}$. A second pulse later aligns the spin vector with the y-axis, allowing the system to resume its oscillatory dynamics. Again, the maximum of $\langle\sigma_z\rangle$ exceeds the previous norm of the spin vector in the delocalized state between the two pulses.

In this last example, the separation of timescales between system and reservoir is so pronounced that the linear SLN equation (42) with the alternative noise spectrum (34) can be used for effective simulations. The simulations discussed in this subsection have also demonstrated that the SLN approach is capable of performing simulations whose characteristic timescales differ by several orders of magnitude.

5. Conclusions and outlook

A bundle of new numerical simulation strategies is added to the recently introduced stochastic Liouville–von Neumann equations for open quantum systems. First, judicious use has been made of the freedom these equations allow in the choice of complex noise spectra. The resulting noise spectra largely avoid driving the system resonantly, leading to markedly improved numerical performance. Additionally, the normalization of subensembles instead of individual samples improves the stability of the method in a crucial way. Finally, use is made of the separation of timescales between dynamical response (inverse bandwidth) and the thermal timescale, yielding stable and efficient simulations for arbitrarily long times.

Using the spin-boson model as a test bed, these simulation methods have been validated as an efficient approach to the dynamics of open quantum systems. Several examples demonstrate its long-time stability as well as its suitability for problems with disparate timescales extending over several orders of magnitude.

A series of simulation results using pulsed fields to extract information on coherent superpositions suggests that the off-diagonal elements of the reduced density matrix are not a suitable measure of quantum coherence in the spin-boson problem; there appears to be hidden coherence related to the system–reservoir interaction.

Since the stochastic Liouville–von Neumann equations discussed here can be factorized into Schrödinger equations, they can be applied to larger systems without any complications other than those present already for conservative systems. The simple expressions found for the stochastic force operators supports this prospect.

Acknowledgements

It is a pleasure to acknowledge fruitful exchanges on the present topic with Ulrich Weiss, as well as his longstanding commitment as a teacher, mentor and friend. Vital discussions with Hermann Grabert have also helped shape this work. Support of Deutsche Forschungsgemeinschaft under SFB 382 is gratefully acknowledged.

Appendix A. Dynamical transformation of the probability measure

In order to transform the linear dynamics of Eq. (12) into the non-linear norm-conserving form (23) we need to find a set of functions $\xi_t(t')$, $\xi_t^*(t')$, $v_t(t')$, $v_t^*(t')$ such that

$$W\left[\xi_t, \xi_t^*, v_t, v_t^*\right] = W[\xi, \xi^*, v, v^*] \times \exp\left(\mathrm{i}\int_0^t \mathrm{d}t'\, v(t')\bar{r}_{t'}\right), \tag{A.1}$$

and show that the Jacobian determinant of the variable change to the new functions as independent variables of the noise averaging is unity.

Using vector notation $\mathbf{z} = (\xi, \xi^*, v, v^*)$, the probability density W can be formally written as

$$W[\xi,\xi^*,v,v^*] = \frac{1}{N}\exp\left(-\frac{1}{2}\int \mathrm{d}t' \int \mathrm{d}t'' \,\mathbf{z}(t')\mathsf{M}(t'-t'')\mathbf{z}^{\mathrm{t}}(t'')\right), \tag{A.2}$$

where N is a normalization constant. Here the superscript 't' denotes a transposed matrix (not a hermitean adjoint) because the inner product of the underlying space of real functions must be used. The four-by-four matrix $M(t'-t'')$ is related to the noise correlation matrix $\langle \mathbf{z}^{\mathrm{t}}(t)\mathbf{z}(t'')\rangle$ through

$$\int \mathrm{d}\tau\, \mathsf{M}(t'-\tau)\langle \mathbf{z}^{\mathrm{t}}(\tau)\mathbf{z}(t'')\rangle = \delta(t'-t''), \tag{A.3}$$

i.e., $\mathsf{M}(t'-t'')$ is the inverse of the noise correlation matrix. With Eqs. (A.2) and (A.3) it is easy to show that Eqs. (19)–(22) 'complete the square' in the exponent of W.

The additional task of computing the corresponding Jacobian only requires a fairly short calculation. Due to the properties required of the guide trajectory, one finds the simplification

$$J = \begin{vmatrix} \frac{\delta\xi_t}{\delta\xi} & \frac{\delta\xi_t}{\delta\xi^*} & \frac{\delta\xi_t}{\delta v} & \frac{\delta\xi_t}{\delta v^*} \\ \frac{\delta\xi_t^*}{\delta\xi} & \frac{\delta\xi_t^*}{\delta\xi^*} & \frac{\delta\xi_t^*}{\delta v} & \frac{\delta\xi_t^*}{\delta v^*} \\ \frac{\delta v_t}{\delta\xi} & \frac{\delta v_t}{\delta\xi^*} & \frac{\delta v_t}{\delta v} & \frac{\delta v_t}{\delta v^*} \\ \frac{\delta v_t^*}{\delta\xi} & \frac{\delta v_t^*}{\delta\xi^*} & \frac{\delta v_t^*}{\delta v} & \frac{\delta v_t^*}{\delta v^*} \end{vmatrix} = \begin{vmatrix} \frac{\delta\xi_t}{\delta\xi} & 0 & \frac{\delta\xi_t}{\delta v} & 0 \\ \frac{\delta\xi_t^*}{\delta\xi} & 1 & \frac{\delta\xi_t^*}{\delta v} & 0 \\ 0 & 0 & 1 & 0 \\ \frac{\delta v_t^*}{\delta\xi} & 0 & \frac{\delta v_t^*}{\delta v} & 1 \end{vmatrix} = \left|\frac{\delta\xi_t}{\delta\xi}\right|. \tag{A.4}$$

Here the second and fourth column simplify due to conditions (17) and (18) while the third row reflects the fact that v is not shifted.

Now the definition (19) of ξ_t immediately leads to

$$\frac{\delta\xi_t(t')}{\delta\xi(t'')} = \delta(t'-t'') + \int_0^t \mathrm{d}s\, \chi_{\mathrm{R}}(t'-s)\frac{\delta\bar{\boldsymbol{r}}(s)}{\delta\xi(t'')}. \tag{A.5}$$

Because $\chi_{\mathrm{R}}(t'-s)$ is a causal response function and $\delta\bar{\boldsymbol{r}}(s)/\delta\xi(t'')$ vanishes for $t'' \geqslant s$ by construction, the integrand is non-zero only for $t'' < t'$. The integral term in Eq. (A.5) therefore does not enter the determinant, and we find

$$J = \left|\frac{\delta\xi_t}{\delta\xi}\right| = 1. \tag{A.6}$$

References

[1] S. Chakravarty, A.J. Leggett, Phys. Rev. Lett. 52 (1984) 5.
[2] H. Grabert, U. Weiss, P. Hänggi, Phys. Rev. Lett. 52 (1984) 2193.
[3] A.J. Leggett et al., Rev. Mod. Phys. 59 (1987) 1.
[4] U. Weiss, Quantum Dissipative Systems, second ed., World Scientific, Singapore, 1999.
[5] A.J. Leggett, in: G. Grinstein, G. Mazenko (Eds.), Directions in Condensed Matter Physics, vol. 1, World Scientific, Singapore, 1986, p. 187.
[6] P. Esquinazi (Ed.), Tunneling in Solids, Springer, Berlin, 1998.
[7] Y. Makhlin, G. Schön, A. Shnirman, Rev. Mod. Phys. 73 (2001) 357.
[8] I. Chiorescu, Y. Nakamura, C.J.P.M. Harmans, J.E. Mooij, Science 299 (2003) 1869.
[9] P. Fendley, F. Lesage, H. Saleur, J. Stat. Phys. 85 (1996) 211.
[10] H. Baur, A. Fubini, U. Weiss, cond-mat/0211046v1, unpublished.
[11] A. Schmid, Phys. Rev. Lett. 51 (1983) 1506.
[12] C.L. Kane, M.P.A. Fisher, Phys. Rev. Lett. 68 (1992) 1220.
[13] J.T. Stockburger, Phys. Stat. Solid 237 (2003) 146.
[14] R.P. Feynman, F.L. Vernon, Ann. Phys. (N.Y.) 24 (1963) 118.
[15] R. Egger, C.H. Mak, Phys. Rev. B 50 (1994) 15210.
[16] K. Leung, R. Egger, C.H. Mak, Phys. Rev. Lett. 75 (1995) 3344.
[17] L. Mühlbacher, R. Egger, J. Chem. Phys. 118 (2003) 179.
[18] D.E. Makarov, N. Makri, Chem. Phys. Lett. 221 (1994) 482.
[19] E. Sim, N. Makri, Chem. Phys. Lett. 249 (1996) 224.
[20] M. Thorwart, P. Reimann, P. Hänggi, Phys. Rev. E 62 (2000) 5808.
[21] L. Diósi, N. Gisin, W.T. Strunz, Phys. Rev. A 58 (1998) 1699.
[22] J.T. Stockburger, C.H. Mak, Phys. Rev. Lett. 80 (1998) 2657.
[23] W.T. Strunz, L. Diósi, N. Gisin, Phys. Rev. Lett. 82 (1999) 1801.
[24] J.T. Stockburger, C.H. Mak, J. Chem. Phys. 110 (1999) 4983.
[25] J.T. Stockburger, H. Grabert, Chem. Phys. 268 (2001) 249.
[26] J.T. Stockburger, H. Grabert, Phys. Rev. Lett. 88 (2002) 170407.
[27] I. Percival, Quantum State Diffusion, Cambridge University Press, Cambridge, 1998.
[28] H.-P. Breuer, F. Petruccione, The Theory of Open Quantum Systems, Oxford University Press, Oxford, 2002, p. 625.
[29] R. Kubo, J. Math. Phys. 4 (1963) 174.
[30] H. Kleinert, S.V. Shabanov, Phys. Lett. A 200 (1995) 224.
[31] U. Weiss, H. Grabert, S. Linkwitz, J. Low Temp. Phys. 68 (1987) 213.
[32] D.F. Walls, G.J. Milburn, Quantum Optics, Springer, Berlin, 1994.
[33] R. Schack, A. Schenzle, Phys. Rev. A 44 (1991) 682.
[34] C.W. Gardiner, P. Zoller, in: Quantum Noise: A Handbook of Markovian and non-Markovian Quantum Stochastic Methods with Applications to Quantum Optics, second ed., Springer Series in Synergetics, vol. 56, Springer, Berlin, 2000.
[35] D. Braun, F. Haake, W.T. Strunz, Phys. Rev. Lett. 86 (2001) 2913.